



Influence of Stacking Order on the Structural and Optical Properties of $\text{Cu}_2\text{ZnSnS}_4$ Absorber Layer Prepared from DC-Sputtered Oxygenated Precursors

January S Gwaydi^{1,2*}, Hezekiah B Sawa¹, Egidius R Rwenyagila¹, Nathanael R Komba³, Talam E Kibona⁴, Nuru R Mlyuka¹, Margaret E Samiji¹, Lwitiko P Mwakyusa¹

¹ Department of Physics, University of Dar es Salaam, P.O. Box 35063, Dar es Salaam, Tanzania.

² Department of Physics, University of Dodoma, P.O. Box 338, Dodoma, Tanzania

³ Department of Chemistry, University of Dar es Salaam, P.O. Box 35061, Dar es Salaam, Tanzania.

⁴ Department of Physics, Mathematics, and Informatics, Mkwawa University College of Education, University of Dar es Salaam, P.O. Box 2513, Iringa, Tanzania.

*Corresponding author, e-mail: january.gwaydi@uodom.ac.tz

Received 8 Dec 2023, Revised 9 Mar 2024, Accepted 4 April 2024, Publ. 30 April 2024

<https://dx.doi.org/10.4314/tjs.v50i1.9>

Abstract

Several studies have attempted to overcome the sudden volume expansion of the precursor during sulfurization by the use of oxygen-containing precursors when growing the CZTS absorber. This work demonstrates the influence of precursor stacking orders on the properties of the CZTS thin film absorber layer from DC-sputtered oxygenated precursors for solar cell applications. CZTS absorber layers were prepared from three types of DC-sputtered stacks, namely, Zn-O/Sn/Cu, Sn/Zn-O/Cu, and Sn/Cu/Zn-O. The precursors were sequentially deposited on a soda lime glass (SLG) using DC-magnetron sputtering and annealed in a sulfur and nitrogen ambient. X-ray diffractometry (XRD) and Raman spectroscopy analyses reveal the formation of crystalline kesterite CZTS structure regardless of the precursor stacking order. Atomic force microscope (AFM) analysis showed that CZTS thin films grown from precursor stacks SLG/Zn-O/Sn/Cu and SLG/Sn/Zn-O/Cu had improved morphological properties with densely packed large grains compared to that with stack SLG/Sn/Cu/Zn-O. SLG/Zn-O/Sn/Cu is the best stack among the studied stacking orders since it exhibits large grains in the absorber layer, which is preferential for high-efficiency thin film solar cells. The use of oxygenated precursor with order Sn/Zn-O/Cu promises improved CZTS absorber properties as it exhibits better morphological properties.

Keywords: $\text{Cu}_2\text{ZnSnS}_4$; absorber; oxygenated precursors; stacking order; DC sputtering;

Introduction

Semiconducting materials based on $\text{Cu}_2\text{ZnSnS}_4$ (CZTS), $\text{Cu}_2\text{ZnSnSe}_4$ (CZTSe), and their derivatives having kesterite structure, have recently attracted considerable attention as promising alternatives to the well-established thin film solar cells based on $\text{Cu}(\text{In,Ga})(\text{S,Se})_2$ (CIGS) and CdTe (Sharmin et al. 2020, Akcay et al. 2021, Sawa et al. 2024a). This interest is partly due to the

constituent elements used in this material, that are not listed as critical raw materials (CRM) (Wadia et al. 2009, Hofmann et al. 2018). Furthermore, the kesterite absorbers have demonstrated promising properties such as tunable direct bandgap and high absorption coefficient ($>10^4 \text{ cm}^{-1}$), which make them suitable for high-efficiency solar cells (Katagiri et al. 2001, Tibaijuka et al. 2018, Akcay et al. 2019). This means that kesterites

are promising material candidates for the fabrication of highly efficient, cost-effective, and environmentally benign thin film solar cells.

Despite the promise and significant effort put into their synthesis, $\text{Cu}_2\text{ZnSn}(\text{SSe})_4$ (CZTSSe)-based solar cells have achieved a record efficiency of 12.6%, which is still far less as compared to that of its counterpart CIGS and CdTe with efficiencies up to $(23.35 \pm 0.5)\%$ and $(21.0 \pm 0.4)\%$, respectively (Green et al. 2023). For pure sulfide kesterite (CZTS)-based solar cells, the efficiency $(11.4 \pm 0.3\%)$ is even lower compared to that of the CZTSSe-based solar cells (Green et al. 2023). Several studies have shown that the synthesis of kesterite absorber mixed with secondary phases, which act as recombination centres that lower the open-circuit voltage (V_{OC}), is among the major problems narrowing the efficiency gap of kesterite-based solar cells (Mwakyusa et al. 2019, Islam et al. 2021, Mwakyusa et al. 2021). Therefore, dedicates the need to understand and establish a controlled synthesis process for making a kesterite absorber in a way that can limit the formation of secondary phases.

The kesterite absorber layer can be prepared by a two-step process in which, (i) the precursor is deposited by either a wet-chemical approach (Tibajuka et al. 2018) or by a vacuum-based approach (Ratz et al. 2019), and then, (ii) annealed at high temperature in a high-pressure chalcogen atmosphere (Gao et al. 2016). The high-temperature annealing provides enough thermal energy that is needed to drive the solid-state reaction, which enhances crystallization and grain growth in the kesterite absorber (Delbos 2012). On the other hand, a high-pressure chalcogen atmosphere suppresses the decomposition of the absorber at the surface (Weber et al. 2010, Delbos 2012, Gao et al. 2016). However, high-temperature annealing is expected to cause detrimental modification of the absorber layer. This includes morphological change (Clark et al. 2017, Özdal et al. 2021), composition shift (Weber et al. 2010), hole-like spots (Yoo et al. 2012, Fairbrother et al. 2014a), delamination (Kim et al. 2022), cracks (Thota et al. 2019)

and blisters (Kim et al. 2022). The delamination, cracks, and blisters have been associated with compression stress and adhesion during the annealing process (Bras et al. 2015, Kim et al. 2022). The compressive stress is attributed to the volume expansion during high-temperature annealing. This problem is more pronounced when metallic precursors are utilized (Yoo et al. 2012, Fairbrother et al. 2014a, Thota et al. 2019). The cracks and hole-like spots may create shunting paths in the final solar cell devices (Malerba et al. 2016, Yang et al. 2017).

Besides, CZTS absorber fabricated from sulfide-stacked structures has been shown to possess promising properties. For example, Olgar et al. (2021) reported the improved structural and optical properties of CZTS films formed from CuSn/ZnS/Cu over those from CuSn/Zn/Cu precursor. This could be interpreted as the presence of chalcogen in the precursor reducing compressive stress and eventually the volume expansion during annealing. Similarly, it has been reported that oxygen-containing precursors inhibit sudden volume expansion during sulfurization (Ishino et al. 2013, Chen et al. 2015, Chen et al. 2016). In addition, the use of oxygen-containing precursors could reduce the compositional deviation of thin film components due to the relatively high-temperature stability of oxides compared to their sulfide counterparts (Chen et al. 2015).

Several studies have attempted to overcome the sudden volume expansion of the precursor during sulfurization by the use of oxygen-containing precursors when growing the CZTS absorber. Ishino et al. (2013) reported improved morphology of CZTS absorber from CZT-O precursors compared to that of CZT precursors. Similarly, Li et al. (2020) reported the improved morphological properties of CZTS absorber grown from the CZT-O precursors deposited by RF magnetron sputtering of ZnO, SnO_2 , and Cu targets in a sequence of $\text{ZnO/SnO}_2/\text{Cu}$. Despite the potential of oxygen inclusion in these precursors, the influence of stacking order on the properties of CZTS absorbers prepared from DC-sputtered oxygenated precursors is not yet fully exploited. This work investigated

the influence of the stacking orders of DC-sputtered oxygenated precursors on the structural, morphological, and optical properties of CZTS absorbers for solar cell application. The oxygenated precursors stacking order was found to have a significant impact on the CZTS absorber properties. Absorber with stacking order; SLG/Zn-O/Sn/Cu showed a larger grain size, high absorption coefficient, and direct bandgap suggesting that absorbers fabricated based on this approach could improve the efficiency of the CZTS-based solar cells.

Materials and Methods

Fabrication of CZTS Thin Films

CZT-O precursors with three different stacking orders as depicted in Figure 1, were deposited on the ultrasonically cleaned soda lime glass (SLG) substrates each with dimensions of 76 mm × 26 mm × 1 mm by direct current (DC) magnetron sputtering in a

BALZERS BAE 250 coating system. Before deposition, the system was evacuated to a base pressure of 6.0×10^{-6} mbar. The precursors were sequentially deposited from the Zn, Sn, and Cu sputtering targets each with 99.99% purity (Plasmaterials Inc, CA, USA). To deposit the Zn-O layer, the Zn target was sputtered in an atmosphere containing Ar and O₂ gases whose flow rates were fixed at 50 sccm and 3.0 sccm, respectively. The deposition temperature and working pressure were set at 150 °C and 6.0×10^{-3} mbar, respectively. The metallic layers of Sn and Cu were deposited at room temperature utilizing the sputtering power of 100 W. The deposition time was 12 min for Zn-O, 7 min for Sn, and 8 min for Cu, achieving the respective thicknesses of 200 nm, 287 nm, and 185 nm adapted from our previous work (Sawa et al. 2018).

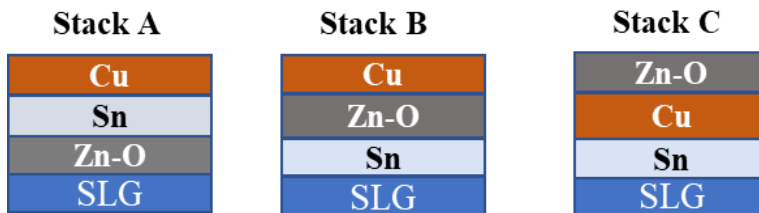


Figure 1: Schematic illustration of the precursor stacking orders.

To prepare the CZTS absorber, the as-deposited CZT-O precursors were thermally annealed in a sulfur and N₂ atmosphere using a rapid thermal processing furnace (RTP – 1000D4). Sulfur pellets of 210 mg and SLG of 2 cm × 2 cm with CZT-O precursor were placed in a semi-sealable graphite box and then inserted in a quartz tube of the furnace. Before annealing, the furnace was evacuated to a base pressure of about 10^{-2} mbar and then filled with N₂ at a flow rate of 80 ml/min for 20 min to obtain a background pressure of about 300 mbar. The furnace was ramped from room temperature to 540 °C with a ramping rate of 140 °C/min, then held at this temperature for 10 minutes, after which, it was allowed to cool naturally. For consistency, all precursor samples were sulfurized under the

same conditions to form a CZTS absorber layer.

CZT-O and CZTS Samples Characterization

The thicknesses of individual layers, CZT-O stacked precursor, and CZTS absorber were determined using the Alpha step IQ surface profiler at a stylus force of 16.4 mg and a scan rate of 50 μm/s. X-ray diffraction (XRD) measurement was carried out using multipurpose Rigaku Ultima IV with Cu-Kα ($\lambda = 1.540629$ Å) line operated at 40 mA and 40 kV. Operated in Bragg-Brentano geometry, samples were scanned in the range of $10^\circ \leq 2\theta \leq 80^\circ$. The crystalline phases were analyzed by comparing the measured XRD patterns with the cards provided by ICDD as described by Mwakyusa et al. (2021).

To confirm the presence of the kesterite phase, the Raman spectroscopy was carried out using a Laser-Raman microscope (Nano-Photon Raman Touch) at an excitation wavelength of 532 nm. The surface morphology of the CZTS thin films was investigated using a Veeco/Bruker Nanoscope IIIa Multimode Atomic Force Microscopy (AFM) in a tapping mode as described by Sawa et al. (2024b). The obtained images were further analyzed with version 5.0 of the WSxM software package (Horcas et al. 2007) and Gwyddion software as described by Nečas and Klápetek (2012). The optical transmittance was measured using a UV-VIS-NIR double-beam spectrophotometer (Perkin Elmer Lambda 1050+) in the wavelength (λ) range $300\text{ nm} \leq \lambda \leq 2000\text{ nm}$ at room temperature. The obtained data were used to determine the optical absorption coefficient and the bandgap of the samples.

Results and Discussions

Structural Properties

To understand the influence of the precursor stacking order on the structural properties of the CZTS absorber, the material phases present in the precursors were first investigated. The XRD pattern (Figure 2) indicated that precursor stacks contained the alloys of Cu_3Sn (ICDD No. 01-1240) and CuSn (ICDD No. 06-0621) together with elemental Sn (ICDD No. 04-0673). This suggests that Sn intermixed with Cu during precursor deposition to form those alloys. Compared to the rest of the stacks, Zn-O/Sn/Cu indicated relatively stronger XRD intensities related to Cu_3Sn and CuSn phases (see Figure 2 [black line]). This suggested that alloying occurs for this stack to a significant extent even at room temperature. No elemental Cu was detected for this stack indicating that all Cu reacted with Sn to form Cu-Sn alloys. Moreover, as illustrated in Figure 2 (black line), the phases related to ZnO were detected. Interestingly, no brasses (Cu-Zn) phases were observed suggesting that the

presence of the ZnO phase prevents the formation of the brasses.

For the Zn-O layer in the middle of Sn and Cu (Sn/Zn-O/Cu), the XRD peak intensities of bronzes (Cu_3Sn and CuSn) significantly decrease. However, the presence of bronzes indicates that partly Sn diffuses toward the surface and reacts with Cu to form Cu-Sn alloys. As can be seen in Figure 2 (red line), the XRD peak at 31.0° corresponding to Sn (Figure 2 (black line)) vanished and the peak at 31.6° corresponding to SnO_2 (ICDD No. 50-1429) evolved (Figure 2 [red line]). This reveals that part of Sn reacted with O_2 to form SnO_2 during the deposition of the Zn-O layer as also reported earlier by Sardashti et al. (2015). The XRD peaks related to the ZnO phase significantly decreased likely because it was somewhat masked by the SnO_2 phase. Moreover, the significant decrease in peak intensities for Cu_3Sn and CuSn suggests that the Zn-O layer prevented the intermixing of Sn and Cu to form those alloys.

When the Zn-O layer is at the top (Sn/Cu/Zn-O), only the Cu_3Sn phase was observed suggesting that deposition temperature likely suppressed the formation of CuSn alloy when the Zn-O layer was deposited on Sn/Cu precursors. Furthermore, the XRD results showed a peak at 42.7° which corresponds to Cu_2O while there were no XRD peaks related to elemental Cu. This indicates that part of Cu reacted with O_2 to form Cu_2O . Perhaps, Cu reacted with residual O_2 in a sputtering chamber to form the CuO_2 phase as the Zn-O layer was deposited immediately after the Cu layer. These findings suggest that stacking orders of the oxygenated metallic precursors can alter CZTS absorber formation pathways and hence significantly influence the quality of the absorber layers. However, along with the order of layers, it is not clear whether or to what extent Sn and Cu-based oxides formed in CZT-O precursors of stacks B and C, respectively, also contribute to the absorber properties.

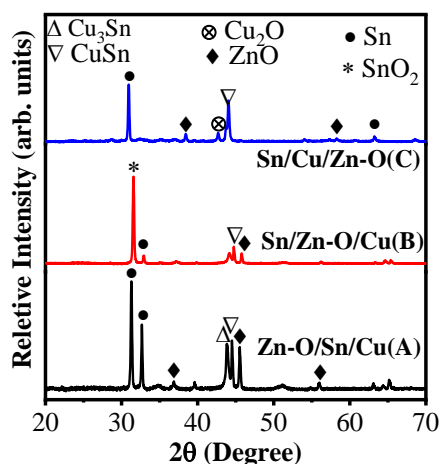


Figure 2: The XRD spectra of the CZT-O precursors with stacks A (Zn-O/Sn/Cu), B (Sn/Zn-O/Cu), and C (Sn/Cu/Zn-O).

Figure 3 (a) depicts XRD patterns of CZTS thin films prepared by sulfurizing precursors with different stacking orders. All samples possess sharp and strong diffraction peaks at 2θ angles of 28.9° , 47.8° and 56.5° that correspond to the respective (112), (220), and (312) crystal planes of tetragonal CZTS compound (ICDD No. 26-0575). Regardless of different precursor stacking orders, all samples exhibited XRD peaks at 26.9° and 34.4° which can be assigned to the CuS secondary phase (ICDD No. 12-0174).

The CZTS absorber layer prepared from stack B with Sn/Zn-O/Cu stacking order possesses an additional small XRD peak at 28° which corresponds to the SnS₂ secondary phase (ICDD No. 40-1467). Based on this result, it can be inferred that the Zn-O layer blocks intermixing of Cu and Sn to form metal alloys as also observed for this precursor (Figure 2 (red line)). The presence of SnS₂ in Sn/Zn-O/Cu stack samples suggests an incomplete reaction. As a result, the CZTS formation proceeds via competition pathways between binaries and ternaries. In the CZTS and its sister materials based on CZTSe thin films, it has been experimentally proven that at low temperatures ternary phase Cu₂SnS(e)₃ reacts with ZnS(e) to form the CZTS(e) phase while at high temperatures via reaction of binary phases (Jung et al. 2017, Mwakyusa et al. 2021).

However, in agreement with earlier reports by Fernandes et al. (2009) and Nakayasu et al. (2017), secondary phases such as Cu₂SnS₃ (CTS) and ZnS could not be distinguished from the CZTS phase using XRD since they have similar lattice parameters. As a result, we used Raman measurement to determine the presence of vibration modes for the CZTS phase in the samples and any other accompanied phases. Figure 3 (b) shows in all samples with different precursor stacking orders, strong vibrational modes located at 338 cm^{-1} and 288 cm^{-1} which corresponded to the CZTS phase (Abusnina et al. 2015, Yang et al. 2017, Sharmin et al. 2020). The Raman spectra indicated the formation of single-phase CZTS thin films with no secondary phases detected. This observation is contrary to the XRD results which showed for all samples, the presence of Cu-S-related secondary phases, and SnS₂ secondary phase to the stack Sn/Zn-O/Cu samples. This observation suggests that the secondary phases were formed deeper in the sample for the Raman to detect as Raman spectroscopy is a surface-sensitive measurement technique that can only probe nearly 100 nm deeper from the surface with green excitation (532 nm) (Mwakyusa 2019). Therefore, the existence of secondary phases masked in the bulk of the CZTS thin films cannot be excluded in this work.

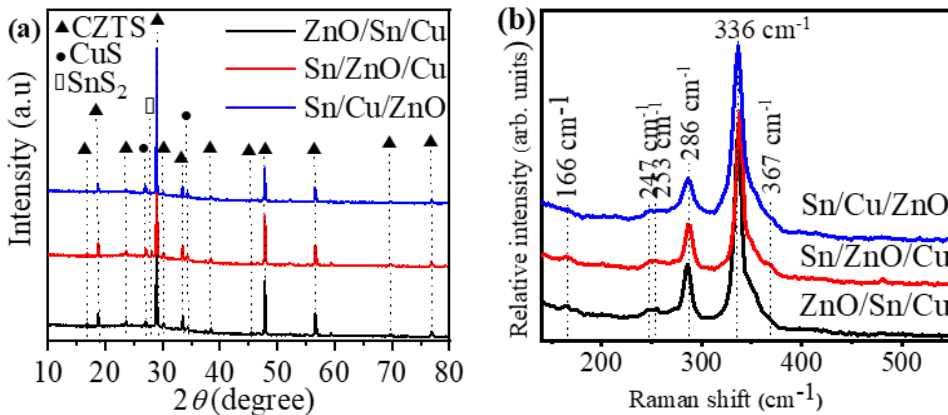


Figure 3: The XRD (a) and Raman spectra (b) for the CZTS absorber prepared from the oxygenated metallic precursors with stacks A, B, and C.

Surface Morphology Properties

It is well acknowledged that the crystallinity of the CZTS absorber can be associated with an increase in grain size. To gain insights into the grain size of the samples, the surface morphology of the absorber was studied from AFM images. The average grain sizes respective to stacks A (Zn-O/Sn/Cu), B (Sn/Zn-O/Cu), and C (Sn/Cu/Zn-O) were found to be 751 nm, 904 nm, and 741 nm as depicted in Table 1. Based on the precursor’s configuration, it appears that absorbers prepared from stack A have more potential for photovoltaic application. It is also known that surface roughness has an impact on the CZTS

solar cell performance as it can affect absorber/buffer layer interface quality. The average surface roughness, root mean square roughness and average grains’ height of the CZTS absorber prepared from different configurations were evaluated. The absorber layer prepared from stack A showed an average roughness of about 83.70 nm while those prepared from stacks B and C had an average roughness of about 68.26 nm and 69.89 nm, respectively. As expected, a similar trend was observed for root mean square and average height (Table 1).

Table 1: The surface morphology parameters for CZTS thin films with stacks A, B and C

Samples	Average grain size (nm)	RMS roughness (R_q) (nm)	Mean roughness (R_a) (nm)	Skewness (S_{sk})	Kurtosis (S_k)
Stack A	751	111.6	83.7	-0.75	1.90
Stack B	904	90.9	68.3	-0.48	2.78
Stack C	740	91.7	69.9	0.01	1.34

Figure 4 (A3, B3, C3) displays the histograms of grain distribution in the CZTS absorber. Stacks A and B showed a very sharp histogram compared to stack C. This suggests that the absorber prepared from stacks A and B possesses mono-dispersed grain distribution (Kumar and Singh, 2020). The presence of Cu on top in stacks A and B promotes the formation of Cu-S phases which are expected

to enhance the diffusion and distribution of chalcogen resulting in improved grain growth and redistribution (Thota et al. 2019). The CZTS samples with a Zn-O layer on top (stack C) showed slightly poor morphology with large voids and small grains. This may be attributed to the presence of ZnO which serves as a thermally insulating layer, as a result preventing sulfur diffusion during the

sulfurization process hence causing less likely grain growth (Fairbrother et al. 2014b).

The 2-D and 3-D AFM images (Figure 4 (A1, B1, C1) and (A2, B2, C2)) also show that the surface is fully covered by diverse peaks of grains as well as valleys. To show the distribution of heights and valleys, the kurtosis and skewness values were determined and listed in Table 1. The kurtosis is the measure

of the sharpness of the peaks at the surface, and skewness indicates the presence of peaks or valleys on the surface. The skewness values indicated that the surfaces of CZTS samples from stacks A and B are mainly composed of valleys (negative values). This is in good agreement with the presence of the large round grains in these samples.

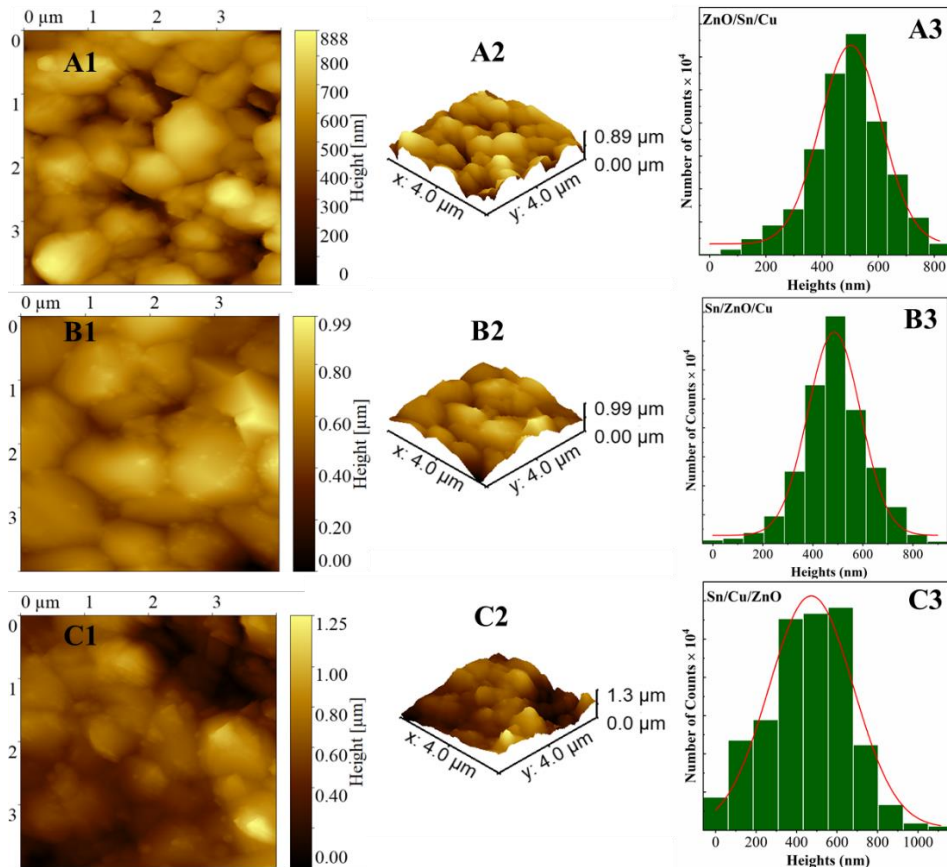


Figure 4: The topography (A1, B1 & C1), 3D images (A2, B2 & C2), and grains distribution (A3, B3 & C3) of CZTS grown from stacks A, B, and C, respectively

Optical Absorption and Bandgap Properties

It is also known that optical absorption is an important factor for a material to be used as an absorber layer for solar cell application. The absorption coefficient, α values for CZTS thin films prepared from different stacking orders were computed from optical transmittance, T measurements, and thicknesses, t using Equation 1.

$$\alpha = \frac{1}{t} \ln \frac{1}{T}$$

1

Figure 5 (a) displays the absorption coefficient spectra of the CZTS absorber deposited with different stacking orders for the wavelength range $300 \text{ nm} \leq \lambda \leq 2000 \text{ nm}$. All samples displayed a high optical absorption coefficient, α in the order $\sim 10^4 \text{ cm}^{-1}$. These values are promising for application in CZTS-based solar cells and agree with earlier reports (Shin et al. 2011, Tibaijuka et al. 2018, Thota et al. 2019, Akcay et al. 2021).

However, the absorption coefficient spectra of stack C showed an increase in absorption in the wavelength range between 780 and 880 nm. This discrepancy may be attributed to the poor surface morphology of the CZTS samples grown from stack C, which may enhance scattering.

It is well known that, the main issue limiting the performance of kesterite solar cells is the larger V_{OC} -deficit. The bandgap energy of the absorber material plays a critical role in defining the maximum achievable V_{OC} . Thus, to get insight into how these stacks will affect bandgap, the optical bandgap of the CZTS thin films was determined from the absorption data. This was achieved by extrapolating a straight line in a curve $(\alpha h\nu)^2$ against the photon energy $h\nu$ of the Tauc plot to the intercept of the horizontal $h\nu$ axis

(Mkawi et al. 2014), as shown in Figure 5 (b). As can be seen in Figure 5 (b), the bandgap values for the absorbers prepared from stack A, stack B, and stack C were 1.51 eV, 1.53 eV, and 1.44 eV, respectively. All three stacks showed bandgap energy values which are within the desired range of the absorber layer for single-junction thin-film solar cells (Katagiri et al. 2008). These values are in good agreement with the reported CZTS absorbers prepared from oxygen-containing precursors (Chen et al. 2015, Li et al. 2020). The results suggest that the CZTS absorber with promising properties for highly efficient CZTS thin film solar cells may be grown from oxygenated precursors. However, the bandgap of CZTS samples from stack C was slightly lower, which can be attributed to poor surface morphology and crystallinity as confirmed through AFM and XRD measurements.

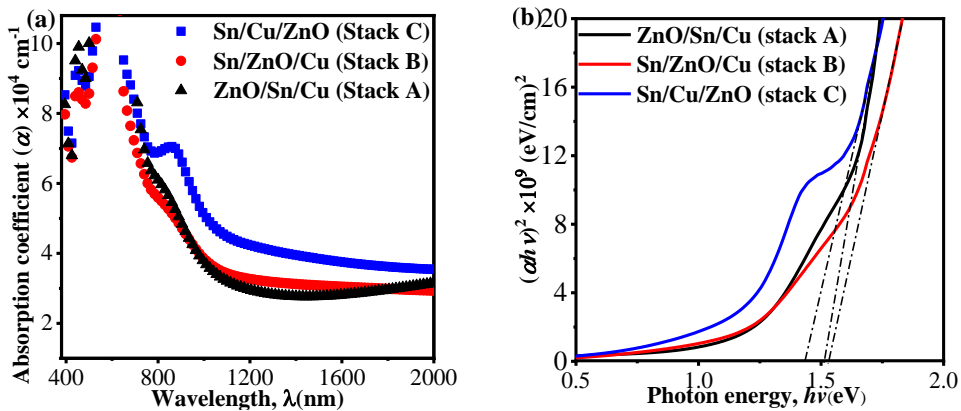


Figure 5: The absorption coefficient spectra (a) and Tauc's plots (b) for the CZTS absorber prepared from precursor stacks A, B, and C.

Conclusions

CZTS absorber layers were prepared by sulfurization of the CZT-O precursors. The influence of stacking orders on the structural and optical properties of the CZTS absorber layers were investigated. The XRD spectra confirmed that all samples, regardless of the precursor stacking orders, had the polycrystalline structure whose dominant peaks represent the CZTS thin films. In addition, the XRD and AFM measurements showed that the crystallinity of CZTS thin films could be improved by changing the order

of stacks of precursor layers. Compared to samples with other stacks, the CZTS absorber prepared from SLG/Zn-O/Sn/Cu precursors demonstrated a larger grain size, which is preferable for solar cell applications. On the other hand, XRD measurements also showed fingerprints of Cu-related secondary phases which could be attributed to the relatively high Cu concentration in the precursors. However, the Raman modes revealed the formation of single-phase CZTS thin films with peaks located at 288 cm^{-1} and 338 cm^{-1} without secondary phases regardless of the precursor

stacking order suggesting that the secondary phases were not formed near the surface of the films. Stacks A (Zn-O/Sn/Cu) and B (Sn/Zn-O/Cu) achieved the direct bandgap energy of ~1.5 eV and absorption coefficients of over 10^4 cm^{-1} which were closer to the ideal values of expected high efficiency CZTS-based thin films solar cells. Stack C with the Zn-O layer on top of the precursors, recorded a slightly lower bandgap of about 1.44 eV, which can be attributed to poor surface morphology and crystallinity of the sample as confirmed through AFM and XRD measurements. Results from this study demonstrated that using the oxygen-containing metallic precursor stacking orders, essentially SLG/Zn-O/Sn/Cu precursors, CZTS absorbers with improved properties can be achieved hence the potential to improve the performance of CZTS solar cells. However, further study to control the elemental percentage composition observed in CZT-O precursors may be required to achieve the potential of these CZTS absorbers.

Acknowledgment

We acknowledge financial support by the University of Dar es Salaam through project grant No. CoNAS-PH22062 as well as MSSEESA network and ISP for research facilities. Appreciation is also extended to LM Majula for XRD and Raman characterization. JS Gwaydi is grateful to the University of Dar es Salaam for the Merit scholarship.

References

- Abusnina M, Matin M, Moutinho HR, Blackburn JL, Alleman J, DeHart C, To B and Al-Jassim M 2015 Suppression of the Cu_{2-x}S secondary phases in CZTS films through controlling the film elemental composition. *IEEE J. Photovoltaics*. 5(5): 1470–1475.
- Akçay N, Gremenok VF, Zaretskaya EP and Özcelik S 2021 Investigation on the properties of $\text{Cu}_2\text{ZnSnSe}_4$ and $\text{Cu}_2\text{ZnSn(S, Se)}_4$ absorber films prepared by magnetron sputtering technique using Zn and ZnS targets in precursor stacks. *Int. J. Energy Res.* 45(2): 2398–2415.
- Akçay N, Zaretskaya EP and Özcelik S 2019 Development of a CZTS solar cell with CdS buffer layer deposited by RF magnetron sputtering. *J. Alloys Compd.* 772: 782–792.
- Bras P, Sterner J and Platzer-Björkman C 2015 Investigation of blister formation in sputtered $\text{Cu}_2\text{ZnSnS}_4$ absorbers for thin film solar cells. *J. Vac. Sci. Technol. A Vacuum, Surfaces, Film.* 33(6): 061201.
- Chen G, Chen S and Huang Z 2016 Preparation of $\text{Cu}_2\text{ZnSnS}_4/\text{Se}_4$ thin films from oxide precursors and its prospect for other Cu_2MSnS_4 thin films. In: Larramendy M and Soloneski S (Eds) *Green Nanotechnology-Overview and Further Prospects*. IntechOpen.
- Chen G, Yuan C, Liu J, Huang Z, Chen S, Liu W, Jiang G and Zhu C 2015. Fabrication of $\text{Cu}_2\text{ZnSnS}_4$ thin films using oxide nanoparticle ink for solar cells. *J. Power Sources*, 276: 145–152.
- Clark JA, Uhl AR, Martin TR and Hillhouse HW 2017 Evolution of morphology and composition during annealing and selenization in solution-processed $\text{Cu}_2\text{ZnSn(S,Se)}_4$. *Chem. Mater.* 29(21): 9328–9339.
- Delbos S 2012 Kesterite thin films for photovoltaics: A review. *EPJ Photovoltaics*, 3: 35004.
- Fairbrother A, Fontané X, Izquierdo-Roca V, Placidi M, Sylla D, Espindola-Rodríguez M, López-Mariño S, Pulgarín FA, Vigil-Galán O, Pérez-Rodríguez A and Saucedo E 2014a Secondary phase formation in Zn-rich $\text{Cu}_2\text{ZnSnSe}_4$ - based solar cells annealed in low pressure and temperature conditions. *Prog. Photovoltaics Res. Appl.* 22(4): 479–487.
- Fairbrother A, Fourdrinier L, Fontané X, Izquierdo-Roca V, Dimitrievska M, Pérez-Rodríguez A and Saucedo E 2014b Precursor stack ordering effects in $\text{Cu}_2\text{ZnSnSe}_4$ thin films prepared by rapid thermal processing. *J. Phys. Chem. C*, 118(31): 17291–17298.
- Fernandes PA, Salomé PMP and da Cunha AF 2009 Growth and Raman scattering characterization of $\text{Cu}_2\text{ZnSnS}_4$ thin films. *Thin Solid Films*. 517(7): 2519–2523.
- Gao C, Schnabel T, Abzieher T, Ahlswede E,

- Powalla M and Hetterich M 2016 Preparation of $\text{Cu}_2\text{ZnSnSe}_4$ solar cells by low-temperature co-evaporation and following selenization. *Appl. Phys. Lett.* 108(1): 013901.
- Green MA, Bothe K, Dunlop ED, Yoshita M, Siefert G, Hao X and Kopidakis N 2023 Solar cell efficiency tables (version 62). *Prog. Photovoltaics Res. Appl.* 31: 651–663.
- Hofmann M, Hofmann H, Hagelüken C and Hool A 2018 Critical raw materials: A perspective from the materials science community. *Sustain. Mater. Technol.* 17: e00074.
- Horcas I, Fernández R, Gómez-Rodríguez JM, Colchero J, Gómez-Herrero J and Baro AM 2007 WSXM: A software for scanning probe microscopy and a tool for nanotechnology. *Rev. Sci. Instrum.* 78(1): 013705.
- Ishino R, Fukushima K and Minemoto T 2013 Improvement of $\text{Cu}_2\text{ZnSnS}_4$ thin film morphology using Cu-Zn-Sn-O precursor fabricated by sputtering. *Curr. Appl. Phys.* 13(9): 1861–1864.
- Islam MF, Yatim NM and Hashim@Ismail MA 2021 A review of CZTS thin film solar cell technology. *J. Adv. Res. Fluid Mech. Therm. Sci.* 81(1): 73–87.
- Jung HR, Shin SW, Suryawanshi MP, Yeo SJ, Yun JH, Moon JH and Kim JH 2017 Phase evolution pathways of kesterite $\text{Cu}_2\text{ZnSnS}_4$ and $\text{Cu}_2\text{ZnSnSe}_4$ thin films during the annealing of sputtered Cu-Sn-Zn metallic precursors. *Solar Energy.* 145: 2-12.
- Katagiri H, Ishigaki N, Ishida T and Saito K 2001 Characterization of $\text{Cu}_2\text{ZnSnS}_4$ thin films prepared by vapor phase sulfurization. *Japanese J. Appl. Physics, Part 1 Regul. Pap. Short Notes Rev. Pap.* 40(2A): 500–504.
- Katagiri H, Jimbo K, Yamada S, Kamimura T, Maw WS, Fukano T, Ito T and Motohiro T 2008. Enhanced conversion efficiencies of $\text{Cu}_2\text{ZnSnS}_4$ -based thin film solar cells by using preferential etching technique. *Appl. Phys. Express.* 1(4): 0412011–0412012.
- Kim SY, Kim SH, Son DH, Yoo H, Kim S, Kim S, Kim YI, Park SN, Jeon DH, Lee J, Jo HJ, Sung SJ, Hwang DK, Yang KJ, Kim DH and Kang JK 2022 Effect of metal-precursor stacking order on volume-defect formation in CZTSSe thin film: Formation mechanism of blisters and nanopores. *ACS Appl. Mater. Interfaces* 14(27): 30649–30657.
- Kumar V and Singh UP 2020 Effect of temperature profile on the formation of CZTSe absorber layer. *Conf. Rec. IEEE Photovolt. Spec. Conf.* 2020-June: 0309–0313.
- Li X, Wang S, Liao H, Yang S, Li X, Wang T, Li J, Li Q and Liu X 2020 The preparation of $\text{Cu}_2\text{ZnSnS}_4$ thin film solar cell based on oxygen containing precursor. *J. Mater. Sci. Mater. Electron.* 31(21): 19309–19317.
- Malerba C, Valentini M, Azanza-Ricardo CL, Rinaldi A, Cappelletto E, Scardi P and Mittiga A 2016 Blistering in $\text{Cu}_2\text{ZnSnS}_4$ thin films: correlation with residual stresses. *Mater. Des.* 108: 725–735.
- Mkawi EM, Ibrahim K, Ali MKM, Farrukh MA and Allam NK 2014 Influence of precursor thin films stacking order on the properties of $\text{Cu}_2\text{ZnSnS}_4$ thin films fabricated by electrochemical deposition method. *Superlattices Microstruct.* 76: 339–348.
- Mwakyusa LP, Jin X, Müller E, Schneider R, Gerthsen D, Rinke M, Paetzold UW, Richards BS and Hetterich M 2021 Phase evolution during annealing of low-temperature co-evaporated precursors for CZTSe solar cell absorbers. *J. Appl. Phys.* 129(15): 153104.
- Mwakyusa LP, Neuwirth M, Kogler W, Schnabel T, Ahlswede E, Paetzold UW, Richards BS and Hetterich M 2019 CZTSe solar cells prepared by co-evaporation of multilayer Cu-Sn/Cu,Zn,Sn,Se/ZnSe/Cu,Zn,Sn,Se stacks. *Phys. Scr.* 94(10): 105007.
- Mwakyusa LP 2019 *Development and Characterization of Co-evaporated CZTSe solar cells.* PhD thesis, Karlsruhe Institute of Technology.
- Nakayasu Y, Tomai T, Oka N, Shojiki K, Kuboya S, Katayama R, Sang L, Sumiya M and Honma I 2017 Fabrication of $\text{Cu}_2\text{ZnSnS}_4$ thin films using a Cu-Zn-Sn-O

- amorphous precursor and supercritical fluid sulfurization. *Thin Solid Films*. 638: 244–250.
- Nečas D and Klapeček P 2012 Gwyddion: An open-source software for SPM data analysis. *Cent. Eur. J. Phys.* 10(1): 181–188.
- Ölğar MA, Sarp AO, Seyhan A and Zan R 2021 Impact of stacking order and annealing temperature on properties of CZTS thin films and solar cell performance. *Renew. Energy* 179: 1865–1874.
- Özdemir T, Chtouki T, Kavak H, Figa V, Guichaoua D, Erguig H, Mysliwiec J and Sahraoui B 2021 Effect of annealing temperature on morphology and optoelectronics properties of spin-coated CZTS thin films. *J. Inorg. Organomet. Polym. Mater.* 31(1): 89–99.
- Ratz T, Brammertz G, Caballero R, León M, Canulescu S, Schou J, Gütay L, Pareek D, Taskesen T, Kim DH, Kang JK, Malerba C, Redinger A, Saucedo E, Shin B, Tampo H, Timmo K, Nguyen ND and Vermang B 2019 Physical routes for the synthesis of kesterite. *J. Phys Energy*. 1(4): 042003.
- Sardashti K, Haight R, Gokmen T, Wang W, Chang L, Mitzi DB and Kummel AC 2015 Impact of nanoscale elemental distribution in high-performance kesterite solar cells. *Adv. Energy Mater.* 10(5): 1402180.
- Sawa HB, Babucci M, Donzel-Gargand O, Pearson P, Hultqvist A, Keller J, Platzer-Björkman C, Samiji ME and Mlyuka NR 2024a Enhanced performance of $\text{Cu}_2\text{ZnSnS}_4$ based bifacial solar cells with FTO and W/FTO back contacts through absorber air annealing and Na incorporation. *Solar Energy Materials and Solar Cells*, 264: 112605.
- Sawa HB, Babucci M, Keller J, Platzer-Björkman C, Samiji ME and Mlyuka NR 2024b Toward improving the performance of $\text{Cu}_2\text{ZnSnS}_4$ based solar cells with Zr, W or sulfurized layers at the $\text{SnO}_2/\text{Cu}_2\text{ZnSnS}_4$ rear interface. *Thin Solid Films*, 793: 140276.
- Sawa HB, Samiji ME and Mlyuka NR 2018 Effects of selenized dc sputtered precursor stacking orders on the properties of $\text{Cu}_2\text{ZnSnSe}_4$ absorber layer for thin film solar cells. *Tanz. J. Sci.* 44(4): 1–11.
- Sharmin A, Bashar MS, Sultana M and Al Mamun SMM 2020 Sputtered single-phase kesterite $\text{Cu}_2\text{ZnSnS}_4$ (CZTS) thin film for photovoltaic applications: Post annealing parameter optimization and property analysis. *AIP Adv.* 10(1): 015230.
- Shin SW, Pawar SM, Park CY, Yun JH, Moon J, Kim JH and Lee JY 2011 Studies on $\text{Cu}_2\text{ZnSnS}_4$ (CZTS) absorber layer using different stacking orders in precursor thin films. *Sol. Energy Mater. Sol. Cells*. 95(12): 3202–3206.
- Thota N, Gurubhasker M, Sunil MA, Prathap P, Subbaiah YP and Tiwari A 2019 Effect of metal layer stacking order on the growth of $\text{Cu}_2\text{ZnSnS}_4$ thin films. *Appl. Surf. Sci.* 396: 644–651.
- Tibaijuka JJ, Samiji ME and Mlyuka NR 2018 Optimization of zinc to tin ratio in a sol gel precursor solution on the growth and properties of annealed CZTS thin films. *Tanzania J. Sci.* 44(4): 36–50.
- Wadia C, Alivisatos AP and Kammen DM 2009 Materials availability expands the opportunity for large-scale photovoltaics deployment. *Environ. Sci. Technol.* 43(6): 2072–2077.
- Weber A, Mainz R and Schock HW 2010 On the Sn loss from thin films of the material system Cu-Zn-Sn-S in high vacuum. *J. Appl. Phys.* 107(1): 013516.
- Yang M, Ma X, Jiang Z, Li Z, Liu S, Lu Y and Wang S 2017 The $\text{Cu}_2\text{ZnSnS}_4$ solar cell with high open circuit voltage. *Phys. B Condens. Matter*. 509: 50–54.
- Yoo H, Kim J and Zhang L 2012 Sulfurization temperature effects on the growth of $\text{Cu}_2\text{ZnSnS}_4$ thin film. *Curr. Appl. Phys.* 12(4): 1052–1057.